第 29 卷 第 11 期
2008 年 11 月

焊 接 学 报
TRANSACTIONS OF THE CHINA WELDING INSTITUTION

Vol. 29 No. 11
November 2008

全熔透 GTAW 熔池表面变形数值分析精度的改进

赵 明， 翟 磊， 孙永兴
（中国石油大学 机电工程学院，山东 青岛 266555）

赵 明

摘 要：针对全熔透 GTAW 熔池表面变形数值模型存在的熔池上、下表面变形耦合作用不确定、重力势能项不完善的问题，做出了相应的改进。以完备的全熔透熔池上、下表面变形方程为基础，基于精度更高的熔池形状数值分析结果，计算和讨论了 GTAW 焊接不锈钢和低碳钢的焊接过程达到准稳态时熔池上表面和下表面的变形，并对计算结果给予了试验验证。解决了已有文献中熔透熔池表面变形计算值偏小的问题，提高了熔池表面变形的数值分析精度。

关键词：表面变形；全熔透熔池；精度改进；数值模拟
中图分类号：TG444 文献标识码：A 文章编号：0253－360X(2008)11－0021－04

0 序 言

钨极惰性气体保护电弧焊(GTAW)焊接过程中，当工件熔透后，在各种力的作用下熔池表面(正面和背面)产生明显的三维下塌变形[1,2]。熔池表面的变形改变了熔池内的传热条件，熔池的三维形状随之要发生变化；而熔池的形状反过来又影响到熔池的表面变形。这就是说，熔池表面变形和熔池形状之间存在双向耦合作用，是影响焊接质量和效率的关键因素之一。对熔池表面变形以及熔池形状进行数值分析并不断改进其计算精度，具有重要的理论意义和工程实用价值。

目前，关于全熔透熔池的研究存在如下主要问题：(1) 全熔透熔池的下表面变形方程，不是经过具体推导得出的，而是直接根据上表面变形方程扩展而来的，缺乏严谨性和可靠性[3－6]；且这些下表面变形方程中重力势能项的表达形式不一致，上、下表面变形方程中 Lagrange 参数前的符号相同，导致整个熔池的正面变形与背面变形的耦合作用不明确。(2) 熔池表面变形受到熔池形状的影响，而现有模型计算出的熔池形状和表面变形本身都还有待改进(比如熔池尾部后拖小于实测结果，表面下塌量小于试验结果)[7,8]。针对上述两个问题，在改进熔池形状的基础上，进一步提高了熔池表面变形的数值分析精度。

1 熔透熔池表面变形方程的完备性

对于全熔透 GTAW 熔池，如图 1 所示，根据能量守恒原理，熔池势能和表面能的变化量应等于电弧力所做的功，因此有

$$\iint_{\Omega_1-\Omega_2}\rho g\left(\frac{1}{2}\varphi^2-H\varphi\right)\mathrm{d}x\mathrm{d}y+\iint_{\Omega_2}\rho g\left[(\psi-\varphi)\left(H-\frac{\psi+\varphi}{2}\right)-L\psi\right]\mathrm{d}x\mathrm{d}y+\iint_{\Omega_1}\gamma\left(\sqrt{1+\varphi_x^2+\varphi_y^2}-1\right)\mathrm{d}x\mathrm{d}y+\iint_{\Omega_2}\gamma\left(\sqrt{1+\psi_x^2+\psi_y^2}-1\right)\mathrm{d}x\mathrm{d}y=\iint_{\Omega_1}p_a\varphi(x,y)\mathrm{d}x\mathrm{d}y \tag{1}$$

式中：p_a 为电弧压力；γ 为液态金属表面张力；ρ 为液态金属密度；g 为重力加速度；H 为熔池最大深度；L 为工件厚度；Ω_1 为熔池上表面液相线所围成区域；Ω_2 为熔池下表面液相线所围成区域；$\varphi(x,y)$ 为熔池上表面形状函数，其坐标原点是工件上表面与电弧轴线的交点；$\psi(x,y)$ 为熔池下表面形状函数，其坐标原点是工件下表面与电弧轴线的交点。

在不加填充材料的情况下，熔池体积应保持不变。结合质量守恒定律，依据能量最小化原理，对式(1)的求解可转化为泛函在拘束条件下的变分问题。经过一系列的推导和论证[9]，得出熔池上表面的变形方程为

$$p_a-\rho g\varphi-\lambda=-\gamma\frac{(1+\varphi_x^2)\varphi_{yy}-2\varphi_x\varphi_y\varphi_{xy}+(1+\varphi_y^2)\varphi_{xx}}{(1+\varphi_x^2+\varphi_y^2)^{3/2}} \tag{2}$$

收稿日期：2008－06－04
基金项目：国家自然科学基金资助项目(50475131)

熔池下表面的变形方程为

$$\rho g(\psi+L)+\lambda = -\gamma\frac{(1+\psi_x^2)\psi_{yy}-2\psi_x\psi_y\psi_{xy}+(1+\psi_y^2)\psi_{xx}}{(1+\psi_x^2+\psi_y^2)^{3/2}} \quad (3)$$

应满足的拘束条件为

$$\iint_{\Omega_1}\varphi(x,y)\mathrm{d}x\mathrm{d}y = \iint_{\Omega_2}\psi(x,y)\mathrm{d}x\mathrm{d}y \quad (4)$$

式(2)～(4)中：λ 为 Lagrange 参数。当 λ 取值合理时，由式(2)和式(3)计算出来的熔池上、下表面变形函数还要满足拘束条件式(4)。

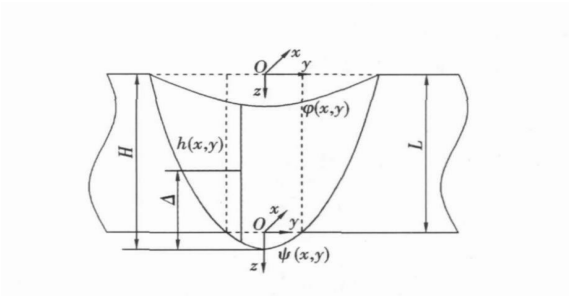

图 1 全熔透熔池横截面示意图

Fig. 1 Schematic drawing for cross section of fully-penetrated molten pool

将式(2)和式(3)与文献[3－8]相比较，发现两点区别：第一，式(2)和式(3)中的 Lagrange 参数 λ 的运算符号分别为“＋”和“－”；而文献中有的相同，有的不同。第二，式(3)左边的第一项是 $\rho g(\psi+L)$，而文献中有的为 $\rho g(\psi+L-\varphi)$，有的为 $\rho g\psi$。

对于上述两点不同，尤其是第二点不同，该如何解释呢？首先，文中 Lagrange 参数 λ 是在数理推导过程中出现的，正确的推导过程确定了其符号在式(2)和式(3)中是不同的；符号不同的 Lagrange 参数 λ 将熔透熔池的上、下表面变形耦合为一个整体。其次，从重力势能项的物理意义来分析，重力势能的大小与参考平面的选取有直接关系；一般来说，零势能参考平面可任意选取，但一经选定，那么所有重力势能在计算过程中都应该以此平面为零势能参考面。从式(3)的推导过程中已知该重力势能项的零势能参考平面为未变形前工件上表面所在的水平面；而从 $\rho g(\psi+L-\varphi)$ 或 $\rho g\psi$ 的表达形式上看，重力势能项的零势能参考平面分别是熔池上表面形状函数 φ 或熔池下表面形状函数 ψ 所在的水平面。而无论对于熔池上表面的形状函数 $\varphi(x,y)$ 或熔池下表面的形状函数 $\psi(x,y)$，即使在同一时刻，不同位置坐标 (x,y) 所对应的 φ 值或 ψ 值也是不同的，因此相关文献中关于重力势能的表达形式不够确切。可见，文中给出的全熔透熔池表面变形的计算公式是正确的、完备的。

对文献[7,8]的另一项改进，是考虑了电弧运动的影响，式(2)中的电弧压力采用了双椭圆分布模式，具体数学表达式见文献[10]。

2 熔池形状计算精度的改进

保证熔池几何形状本身的计算精度，使熔池表面变形方程的求解区域 Ω_1 和 Ω_2 更符合实际，是改进熔池表面变形计算精度的基础和前提。文中采用了改进的全熔透 GTAW 熔池形态数值分析模型[10]。该模型采用电弧热流双椭圆分布模式并正确选取热源在工件上的计算区域，同时采用液体分数法处理相变潜热的影响，使计算得到的熔池上表面形状与试验测试结果吻合良好，提高了 GTAW 熔池形状的数值计算精度，解决了数值计算结果中熔池尾部后拖不足的问题[7]。图 1 是某一工艺条件下熔池形状的计算与测试结果[10]。

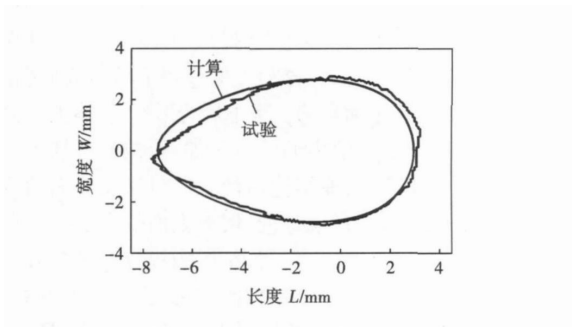

图 2 熔池上表面形状计算结果与试验结果

Fig 2 Comparison between calculated and measured molten pool geometry at top surface

3 数值分析结果

算例 1：GTAW 焊接 3 mm 厚不锈钢板，焊接电流为 100 A，电弧电压为 12 V，焊接速度为90 mm/min。数值计算结果表明，熔池在 0.3 s 时形成，在 4.6 s 时工件全熔透，到 8.0 s 左右焊接过程达到宏观准稳态。图 3 分别从纵向和横向根出了熔池上、下表面变形的计算结果。熔池上表面的最大下塌量为 0.35 mm，熔池下表面的最大下塌量为 0.51 mm。图 4是准稳态时熔池上、下表面的三维变形。

算例 2：GTAW 焊接 3 mm 厚低碳钢板，焊接电流为 120 A，电弧电压为 12 V，焊接速度为 120 mm/min。数值计算结果表明，熔池在 0.2 s 时形

成,在 3.0 s 时工件全熔透,到 5.5 s 左右焊接过程达到宏观准稳态。图 5 中熔池上表面的最大下塌量为 0.64 mm,熔池下表面的最大下塌量为 0.97 mm。图 6 是准稳态时熔池上、下表面的三维变形。

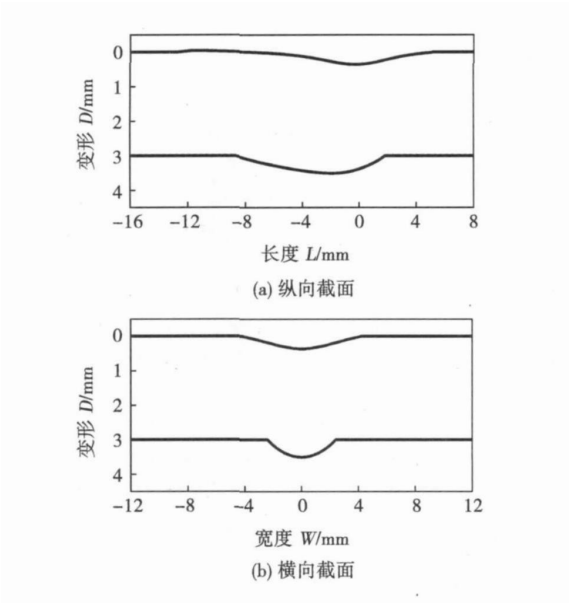

图 3　不锈钢焊接熔池表面的变形

Fig. 3　Molten pool surfaces deformation for welding stainless steel

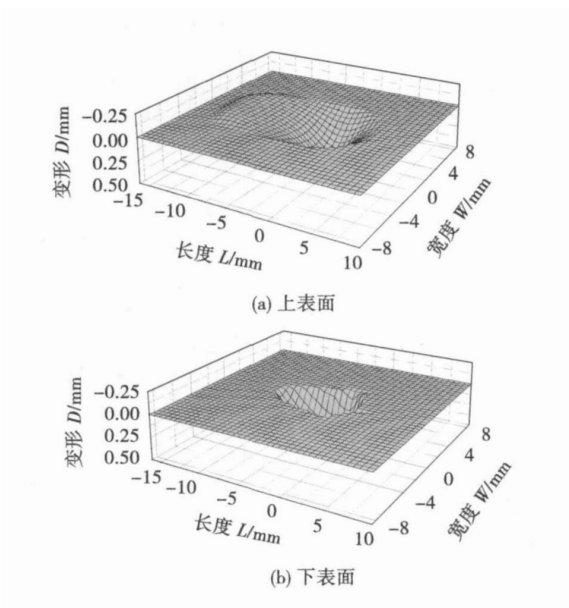

图 4　不锈钢焊接熔池表面变形的三维视图

Fig. 4　Three-dimensional molten pool surfaces deformation for welding stainless steel

从图 4~6 中可见,熔池熔透部分位于熔池的中后部。上表面的最大下塌变形发生在电极正下方,在靠近熔池尾部有轻微的隆起,而下表面的最大下塌变形发生在距离电极一定距离的熔池后部;上表面的下塌区域明显大于下表面的下塌区域,但上表面的下塌程度不如下表面的明显。

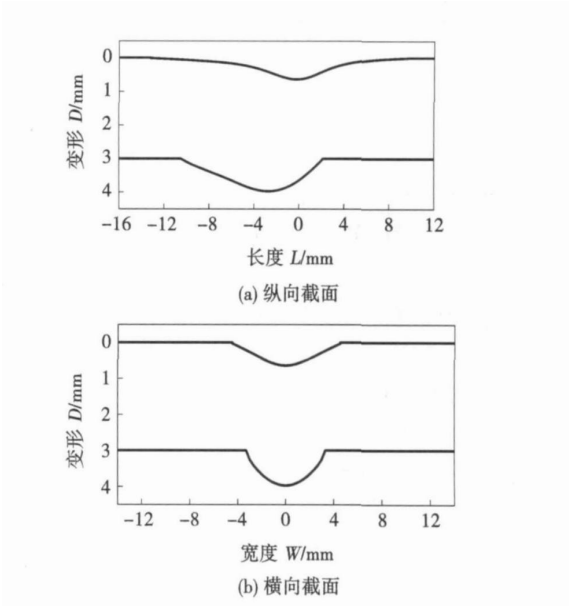

图 5　低碳钢焊接熔池表面的变形

Fig. 5　Molten pool surfaces deformation for welding mild steel

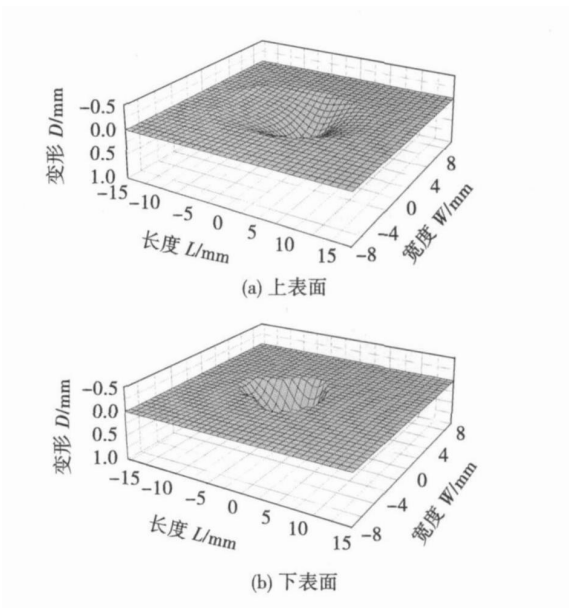

图 6　低碳钢焊接熔池表面变形的三维视图

Fig 6　Three-dimensional molten pool surfaces deformation for welding mild steel

4　验　　证

表 1 是文献[8]的计算结果与文中计算结果的比较。可见,在相同工艺条件下,文中计算得到的熔池自由表面变形量大于文献给出的熔池自由表面变

形量，解决了熔池表面变形计算结果偏小的问题。

表 1 熔池表面最大变形量(mm)

Table 1 Maximum depressed depths of molten pool surfaces

	文献[8]	文中计算结果
上表面最大下塌量	0.12	0.33
下表面最大下塌量	0.24	0.62

熔池表面的下凹变形与焊缝横断面的最大下塌变形有直接对应关系。根据焊缝横截面宏观金相照片，可以测量出焊缝横截面形状(熔合线)以及焊道表面的下凹变形。图 7 对比了焊缝横截面熔合线形状和焊道表面变形的数值计算结果与试验检测结果(GTAW 焊接 3 mm 厚不锈钢板，焊接电流为 125 A，电弧电压为 16 V，焊接速度为 115 mm/min)。由此可见，文中计算得到的焊缝横截面形状和熔池表面变形与试验结果吻合良好。

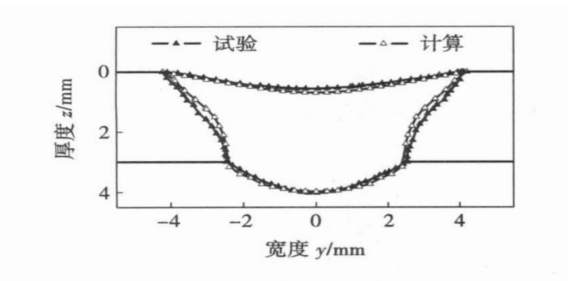

图 7 试验结果和计算结果的比较

Fig. 7 Comparison between calculated and experimental results

5 结 论

(1) 通过与现有文献的对比和分析，论证了直接推导出的全熔透熔池上、下表面变形方程中，Lagrange 参数前的符号应是相异的，重力势能项的表达形式应是 $\rho g(\psi + L)$。

(2) 在全熔透熔池形状计算精度改进的基础上，给出了熔池上、下表面变形的计算结果，解决了已有模型计算得到的熔透熔池表面变形量偏小的问题，并通过试验验证了计算结果的可靠性，提高了全熔透熔池表面变形的数值计算精度。

参考文献：

[1] Choo R T C, Szekely J, Westhoff R C. Modeling of high-current arcs with emphasis on free surface phenomena in the weld pool[J]. Welding Journal, 1990, 69(9): 346s—361s.

[2] Tsai M C, Kou S. Electromagnetic-force-induced convection in weld pools with a free surface[J]. Welding Journal, 1990, 69(6): 241s—246s.

[3] Ohji T, Nishiguchi K. Mathematical modeling of molten pool in arc welding of thin plate[R]. Osaka: Osaka University, 1983.

[4] Wu C S, Dorn L. Prediction of surface depression of a tungsten inert gas weld pool in the full-penetration condition[J]. Journal of Engineering Manufacture, 1995, 209(2): 221—226.

[5] Cao Z N, Zhang Y M, Kovacevic R. Numerical dynamic analysis of moving GTA weld pool[J]. Journal of Manufacture Science and Engineering, 1998, 120(2): 173—178.

[6] Fan H G, Tsai H L, Na S J. Heat transfer and fluid flow in a partially or fully penetrated weld pool in gas tungsten arc welding[J]. International Journal of Heat and Mass Transfer, 2001, 44(2): 417—428.

[7] Zhao P C, Wu C S, Zhang Y M. Numerical simulation of the dynamic characteristics of weld pool geometry with step-change of welding parameters[J]. Modelling and Simulation in Materials Science and Engineering, 2004, 12(5): 765—780.

[8] Zhao P C, Wu C S, Zhang Y M. Modelling the transient behaviours of a fully penetrated gas-tungsten arc weld pool with surface deformation[J]. Journal of Engineering Manufacture, 2005, 219(1): 99—110.

[9] Wu C S. Predicting the deformation of both top and bottom surfaces in completely penetrated weld pool[R]. Jinan: Shandong University, 2005.

[10] Zhao Ming, Li Ruiying. Numerical analysis of dynamic variation of weld pool geometry in fully-penetrated TIG welding[J]. China Welding, 2008, 17(2): 47—53.

作者简介：赵 明，女，1973 年出生，博士。主要研究方向为焊接过程的数值分析。发表论文 10 余篇。

Email: zhaoming08@hdpu.edu.cn

arc in understanding physical property of hyperbaric welding arc and seeking improvement of the quality of underwater hyperbaric welding. The spectral diagnostics was introduced, and the TIG welding arc in high-pressure was analyzed. A set of feasible method of high-pressure arc temperature measurement was established. The welding arc temperature in high-pressure was analyzed, and the function between the environment pressure and the arc temperature was established. The experimental result was analyzed. This research is significant and valuable to the study of hyperbaric welding arc physics.

Key words: arc; hyperbaric welding; temperature; spectral diagnostics

Improvement on numerical analysis precision of surface deformation of molten pool in fully-penetrated GTAW ZHAO Ming, ZHAI Lei, SUN Yongxing (College of Mechanical & Electronic Engineering, China University of Petroleum, Qingdao 266555, China).

Abstract: The improvement was made to solve the problems existing in present numerical models of fully-penetrated GTAW (gas tungsten arc welding) weld pool surface deformation. Based on the complete and correct equations of both top and back surfaces deformations of molten pool and the more accurately predicted weld pool geometry, the fully-penetrated molten pool surface deformation at the quasi-steady state were numerically calculated and discussed. The calculated results were verified by experiments. The results indicate that this study solves the problems of the lesser predicted molten pool surface deformation in literatures, and improves the numerical analysis precision of molten pool surface deformation.

Key words: surface deformation; fully-penetrated molten pool; precision improvement; numerical simulation

Residual distortion of thin-plate weldments controlled by rotating extrusion LI Jun, YANG Jianguo, WENG Lulu, FANG Hongyuan (State Key Laboratory of Advanced Welding Production Technology, Harbin Institute of Technology, Harbin 150001, China).

Abstract: A new technology was proposed to control residual distortion of thin-plate weldments with rotating extrusion. Extrusion force with is exerted by rotary action of an extrusion head on weld and zone near the weld to form the tensile plastic strain, which can counteract the welding-induced residual compressive plastic strain, and reduce or even eliminate the welding residual distortion. The surface of weld processed by this method is flat and smooth, and the stress concentration in the weld is decreased obviously. Experimental results showed that this technology can decrease the welding residual distortion of thin-plate weldments to below 3% of that of conventional weldments. The control effect of welding residual distortion has relation to some technical parameters. A good control effect of welding distortion can be acquired only when all kinds of technological parameters are matched properly.

Key words: rotating extrusion; welding; thin plate; distortion

Effect of supersonic fine particles bombarding on oxidation behavior of MCrAlY coating JI Zhaohui, WANG Minzhuan, FENG Ribao, WANG Zhiping (College of Sciences, Civil Aviation University of China, Tianjin 300300, China).

Abstract: MCrAlY bonding coating was deposited on GH99 high-temperature alloy using atmospheric plasma spraying (APS). The influence of supersonic fine particles bombarding on microstructure and thermally grown oxide of MCrAlY coating was investigated, and the interface, phase constituents and the evolution of the coating exposed at 1 100 ℃ for different times was evaluated by SEM, XRD and glow discharge spectroscopy. The experimental results showed that the oxide particles were fine through supersonic treating, then Al_2O_3 scale formed quickly on MCrAlY surface, and Ni and Cr were prevented from oxidizing. For this reason, the formation of $Ni(Cr,Al)_2O_4$ can be avoided and flaw decreases, so that the high-temperature oxidation resistance of coating is improved.

Key words: thermal barrier coating; supersonic fine particles bombarding; thermally grown oxide; plasma spraying; MCrAlY bond coat

Modeling on weld position and welding torch pose in welding of intersected pipes REN Fushen[1,2], CHEN Shujun[1], YIN Shuyan[1], GUAN Xinyong[1] (1. School of Mechanical Engineering and Applied Electronics Technology, Beijing University of Technology, Beijing 100022, China; 2. School of Mechanical Science and Engineering, Daqing Petroleum Institute, Daqing 163318, Heilongjiang, China).

Abstract: The welding seam of intersected pipes is a typical and complicated space welding seam. The models of weld position and welding torch pose were founded for arc welding robot, and their position and pose were described precisely and quantificationally by coordinates. Then, the welding torch orientations were described by work angle, traveling angle and rotation angle, and the calculation methods were presented. A new simple method of calculation is put forward to establish the coordinate system of welding seam according to the characteristic analysis that any tangent through the point on intersection line coincides with the intersection line of two cylinder sections at this point. The model is general to the intersected pipes and it has significance for modeling on weld position and welding torch pose, simulating and off line programming for robot welding.

Key words: arc welding robot; intersection weld; model of weld position; model of welding torch pose

Analysis on microstructure and high temperature stability of nanostructured thermal barrier coatings WANG Hongying[1], HAO Yunfei[1,2], CHEN Hui[2], TANG Weijie[1] (1. Industry Center, Shenzhen Polytechnic, Shenzhen 518055, Guangdong, China; 2. Material Science and Engineering College, Southwest Jaotong University, Chengdu 610031, China).

Abstract: Nanostructured thermal barrier coatings (TBCs) have been prepared by air plasma spraying using reconstituted nano-